screened with a ^{32}P-labeled probe generated by PCR, with the 210-bp P-opsin cDNA obtained by RT-PCR as template. Filters were hybridized with the probe overnight at 65°C in Church buffer (*13*) and washed at high stringency in 0.2× saline sodium citrate (SSC), 0.5% SDS at 65°C. More than 30 individual partial P-opsin cDNA clones and one full-length clone were obtained (ranging in size from 800 to 1696 bp). Some of the partial clones (~1/3) had the sequence CAG (glutamine) for amino acid 28 rather than TGG (tryptophan). This may be due to a polymorphism in the population or to RNA editing.
13. G. M. Church and W. Gilbert, *Proc. Natl. Acad. Sci. U.S.A.* **81**, 1991 (1984).
14. The probe for Northern blot analysis was made by incorporating [^{32}P]dCTP (deoxycytidine triphosphate) into a 210-bp PCR product by amplifying P-opsin cDNA (amino acids 235 to 305).
15. I. Kyte and R. F. Doolittle, *Biology* **157**, 105 (1982); J. Devereaux, P. Haeberil, O. Smithies, *Nucleic Acids Res.* **12**, 387 (1984). The secondary structure of P-opsin was extrapolated from its hydrophobicity on the basis of a similar plot of bovine rhodopsin (*16*).
16. H. G. Khorana, *J. Biol. Chem.* **267**, 1 (1992).
17. F. F. Davidson, P. C. Loewen, H. G. Khorana, *Proc. Natl. Acad. Sci. U.S.A.* **91**, 4029 (1994).
18. E. M. Ross, *Neuron* **3**, 141 (1989).
19. H. Kühn, *Prog. Retinal Res.* **3**, 123 (1984); U. Wilden, S. W. Hall, H. Kühn, *Proc. Natl. Acad. Sci. U.S.A.* **83**, 1174 (1986).
20. P. J. Dolph *et al.*, *Science* **260**, 1910 (1993).
21. R. R. Franke, T. P. Sakmar, M. Graham, H. G. Khorana, *J. Biol. Chem.* **267**, 14767 (1993).
22. Genomic clone GP3 and others were obtained by screening of a chicken genomic library contained in Lambda Fix II (Stratagene) with a random-primed probe made from the full-length P-opsin cDNA clone. After overnight hybridization at 65°C in Church buffer, filters were washed at high stringency (0.2× SSC, 0.5% SDS, 65°C). Lambda DNA from purified positive plaques was subcloned into pBluescript II KS+, mapped by restriction endonuclease digestion, and sequenced. Both of the genomic clones that were sequenced through this region contain the sequence CAG (glutamine) at amino acid 28 rather than TGG (tryptophan) as found in the majority of cDNAs (*12*).
23. Tree reconstruction was performed as described in figure 3 of (*1*) with PHYLIP version 3.5c, assembled by J. Felsenstein [*Cladistics* **5**, 164 (1989)]. An alignment of sequences was generated by McCAW [M. O. Dayhoff, R. M. Schwartz, B. C. Orcutt, *Atlas of Protein Sequencing and Structure*, M. O. Dayhoff, Ed. (National Bioscience Research Foundation, Washington, DC, 1978), vol. 5, p. 345; G. D. Schuler, S. F. Altschul, D. J. Lipman, *Protein Struct. Funct. Genet.* **9**, 180 (1991)], with minor adjustments made by hand. Distance matrices were calculated with PRODIST, which uses the Dayhoff PAM 001 matrix. NEIGHBOR was used to generate pairwise groupings with the neighbor-joining method described by N. Saitou and M. Nei [*Mol. Biol. Evol.* **4**, 406 (1987)]. Randomization of sequence entry order had no effect on tree reconstruction. Bootstrapping (SEQBOOT) generated multiple (n = 100) randomly resampled data sets from the alignment [J. Felsenstein, *Evolution* **39**, 783 (1985); *Annu. Rev. Genet.* **22**, 521 (1988)]. CONSENSE produced a consensus tree from the data set. No attempt was made to associate branch length with amino acid substitution rate. Similar results were obtained using the accepted-mutation parsimony (AMP) method of Kolakowski and Rice, available by e-mail at lfk@receptor.MGH.Harvard.Edu.
24. J. S. Takahashi, N. Murakami, S. S. Nikaido, B. L. Pratt, L. M. Robertson, *Recent Prog. Horm. Res.* **45**, 279 (1989).
25. J. G. Flannery, W. O'Day, B. A. Pfeffer, J. Horwitz, D. Bok, *Exp. Eye Res.* **51**, 717 (1990).
26. S. Yarfitz and J. B. Hurley, *J. Biol. Chem.* **269**, 14329 (1994).
27. T. Deguchi, *Science* **203**, 1245 (1979); L. M. Robertson and J. S. Takahashi, *J. Neurosci.* **8**, 12 (1988); *ibid.*, p. 22.
28. M. Zatz and D. A. Mullen, *Brain Res.* **453**, 63 (1988).
29. T. Okano, T. Yoshizawa, Y. Fukada, *Nature* **372**, 94 (1994).
30. Abbreviations for the amino acid residues are as follows: A, Ala; C, Cys; D, Asp; E, Glu; F, Phe; G, Gly; H, His; I, Ile; K, Lys; L, Leu; M, Met; N, Asn; P, Pro; Q, Gln; R, Arg; S, Ser; T, Thr; V, Val; W, Trp; and Y, Tyr.
31 We thank L. F. Kolakowski for constructing evolutionary trees by the AMP method, J. Kornhauser and A. Opper for performing in situ hybridization, J. Florez for pineal cell cultures to make ZT 12 cDNA library, and R. Wurzberger for sequencing and oligonucleotide synthesis. Supported by NIH grants MH39592 and EYO8467 to J.S.T., MH10287 to K.J.S., MH10225 to M.M., MH10369 to R.K.B., and EYO4801 to M.L.A.

13 September 1994; accepted 21 December 1994

Massive Cell Death of Immature Hematopoietic Cells and Neurons in Bcl-x–Deficient Mice

Noboru Motoyama,* Fanping Wang,* Kevin A. Roth,* Hirofumi Sawa, Kei-ichi Nakayama, Keiko Nakayama, Izumi Negishi, Satoru Senju, Qing Zhang, Satoshi Fujii, Dennis Y. Loh†

bcl-x is a member of the *bcl-2* gene family, which may regulate programmed cell death. Mice were generated that lacked Bcl-x. The Bcl-x–deficient mice died around embryonic day 13. Extensive apoptotic cell death was evident in postmitotic immature neurons of the developing brain, spinal cord, and dorsal root ganglia. Hematopoietic cells in the liver were also apoptotic. Analyses of *bcl-x* double-knockout chimeric mice showed that the maturation of Bcl-x–deficient lymphocytes was diminished. The life-span of immature lymphocytes, but not mature lymphocytes, was shortened. Thus, Bcl-x functions to support the viability of immature cells during the development of the nervous and hematopoietic systems.

Apoptosis (programmed cell death) is a poorly understood process that occurs in many tissues during early development and throughout adult life in many organisms. The protooncogene *bcl-2*, whose gene product inhibits certain forms of apoptosis (*1*), is widely expressed during mouse development and in long-lived cells such as neurons and stem cells of many tissues in an adult mouse (*2*). Although early embryonic lethality was expected on the basis of its expression pattern, *bcl-2*–ablated mice were shown to remain viable, and major abnormalities were limited to the hair color, polycystic kidney development, and decreased lymphoid cell life-span (*3*, *4*). In particular, the nervous system developed normally. These findings may be attributed to redundancy, because *bcl-2* is only one of a larger family of related genes (*5*, *6*). As expected, other members of the *bcl-2* family can inhibit apoptosis in in vitro assays (*5*, *6*).

bcl-x, a member of the *bcl-2* gene family, can be alternatively spliced to produce two protein isoforms (Bcl-x_L and Bcl-x_S), one of which (Bcl-x_L) inhibits apoptosis (*6*). Bcl-x in mice is expressed highly during development and in the brain, thymus, and kidney in adult, predominantly in the Bcl-x_L form (*7*, *8*). To elucidate the functional and developmental role of Bcl-x, we used homologous recombination in embryonic stem (ES) cells to generate mice lacking both Bcl-x_L and Bcl-x_S (*9*) (Fig. 1). Heterozygous

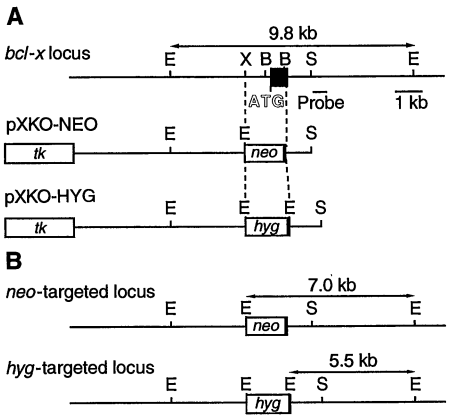

Fig. 1. Target disruption of the *bcl-x* gene (*9*). (**A**) Genomic structure surrounding coding exon of mouse *bcl-x*, and structure of the pXKO-NEO and pXKO-HYG targeting vectors. The position of translation initiation site is shown (ATG). (**B**) Predicted structure of the targeted *bcl-x* locus. The location of the hybridization probe, a 0.4-kb Kpn I–Pst I fragment, and expected sizes of the Eco RV fragments that hybridize with the probe are indicated. B, Bam HI; E, Eco RV; S, Spe I; X, Xho I. The restriction map of Bam HI is not complete.

N. Motoyama, F. Wang, K.-i. Nakayama, K. Nakayama, I. Negishi, S. Senju, Q. Zhang, D. Y. Loh, Howard Hughes Medical Institute and Departments of Medicine, Genetics, and Molecular Microbiology, Washington University School of Medicine, St. Louis, MO 63110, USA.
K. A. Roth, Departments of Pathology, Molecular Biology, and Pharmacology, Washington University School of Medicine, St. Louis, MO 63110, USA.
H. Sawa and S. Fujii, Division of Cardiovascular Medicine, Washington University School of Medicine, St. Louis, MO 63110, USA.

*These authors contributed equally to this report.
†To whom correspondence should be addressed.

mutant mice (*bcl-x*$^{+/-}$) were healthy and normal in size. Homozygous mutant mice (*bcl-x*$^{-/-}$) died around 13 days of gestation (E13) (Table 1).

Embryos from E11.5, 12.5, and 13.5 *bcl-x*$^{-/-}$, *bcl-x*$^{+/-}$, and wild-type mice were histologically examined. E11.5 *bcl-x*$^{-/-}$ mice were histologically similar to heterozygotes and wild-type mice with one major exception. Throughout the brain and spinal cord in the regions containing postmitotic, differentiating neurons, there was extensive cell death. In the most mature regions of the E11.5 nervous system, the rostral spinal cord and brain stem, there were large areas containing pyknotic nuclei, karyorrhectic debris, and frequent phagocytic cells with engulfed debris (Fig. 2). The histologic appearance of the degenerative zones in the *bcl-x*$^{-/-}$ mice resembles that seen in regions of naturally occurring neuronal cell death (*10*); however, the magnitude of cell death and its neuroanatomic distribution exceeds that seen in wild-type and heterozygote littermates.

By E12.5, extensive areas of neuronal degeneration were seen throughout the maturing *bcl-x*$^{-/-}$ brain, including the diencephalon, midbrain, and caudal spinal cord. Although naturally occurring neuronal cell death was seen in E12.5 wild-type and heterozygote mice in regions such as the rostral spinal cord and dorsal root ganglia, there was no evidence of massive, diffuse cell death as seen in the *bcl-x*$^{-/-}$ mice.

The degenerative changes in the *bcl-x*$^{-/-}$ nervous system appeared to be localized to regions of differentiating neurons. Because these mice had already died before mature neuronal phenotypes could be identified by histologic stains, we further characterized the zones of death by microtubule-associated protein 2 (MAP2) immunoreactivity (Fig. 2, F to H). The MAP2 protein is neuron-specific and is expressed during embryonic brain development (*11*). Immunohistochemical staining of E11.5 and 12.5 wild-type and *bcl-x*$^{-/-}$ brain and spinal cord showed that cells in the mitotically active ventricular zone lacked MAP2 immunoreactivity, but that more peripherally located differentiating cells possessed strong MAP2 staining. The vast majority of degenerating cells, identified by bisbenzamide staining, were located in MAP2-positive regions. The identification of the bisbenzamide-positive apoptotic cells in the *bcl-x*$^{-/-}$ nervous system as neurons is further supported by recent in vitro experiments. After 2 days in 2% fetal calf serum containing medium, primary dissociated E12.5 *bcl-x*$^{-/-}$ telencephalic cell cultures contained three times as many condensed or clumped bisbenzamide-labeled nuclei and only 30% of the number of neurofilament heavy chain immunoreactive neurons as heterozygote and wild-type cultures (8). These results also suggest that

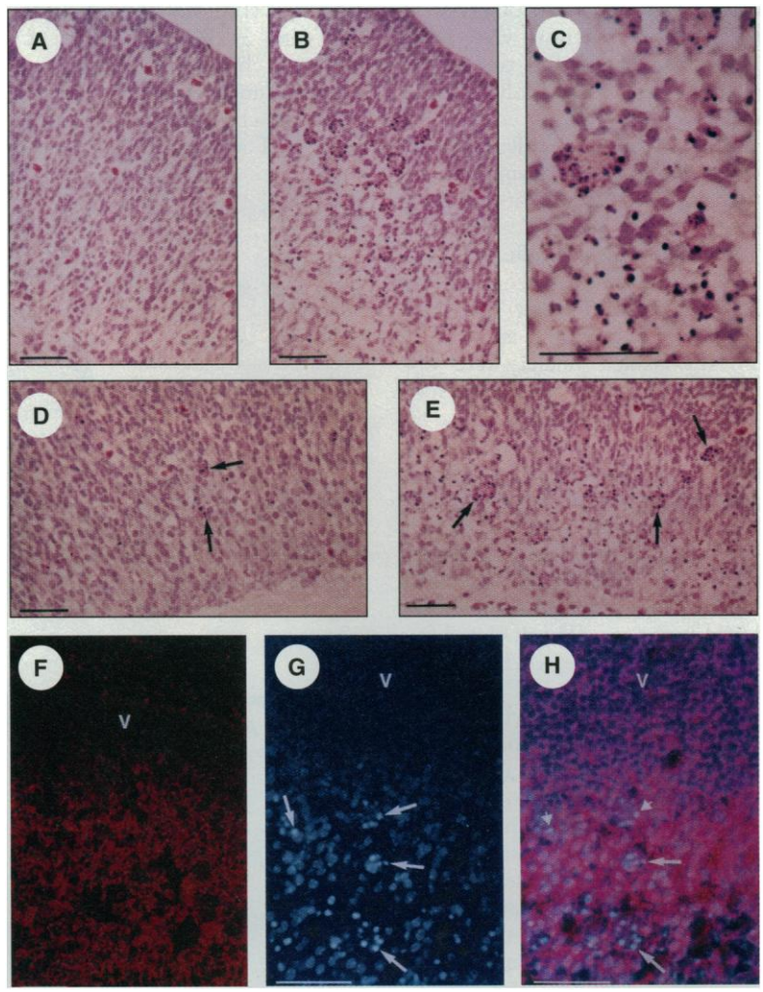

Fig. 2. Histologic appearance of E11.5 wild-type (A and D) and *bcl-x*$^{-/-}$ (B, C, and E) brainstem (A to C) and spinal cord (D and E) (*25*). A hematoxylin-eosin–stained section of the rostral pons from a wild-type mouse (**A**) shows immature neuroepithelial cells adjacent to the fourth ventricle (upper right corner) and ventrally located differentiating cells. A similarly located section from a *bcl-x*$^{-/-}$ animal (**B**) reveals extensive cell death of the differentiating neuroepithelial cells. High magnification (**C**) shows pyknotic nuclei, karryorrhectic debris, and distended phagocytic cells. A sagittal section of the rostral spinal cord from a wild-type mouse (**D**) shows occasional pyknotic nuclei and phagocytic cells in the ventral spinal cord (indicated by arrows). In comparison, the spinal cord of a *bcl-x*$^{-/-}$ mouse (**E**) contains enormous numbers of dead cells and phagocytes. MAP2 immunolabeling (F and H) and bisbenzamide staining (G and H) of E12.5 *bcl-x*$^{-/-}$ brainstem (F to H). The ventricular zone (labeled V) shows little MAP2 immunoreactivity, whereas cells located in the ventral medulla possess strong, bright red–fluorescent MAP2 immunoreactivity (**F**). Bisbenzamide staining (**G**) shows normal diffuse blue fluorescent nuclear staining of the ventricular zone cells (labeled V) and numerous clumped, fragmented, bright blue–white fluorescent nuclei (indicated by arrows) in the ventral medulla. Double exposure of MAP2 immunofluorescence and bisbenzamide labeling (**H**) shows weak MAP2 staining of the densely packed, immature cells of the ventricular zone (labeled V) and strong MAP2 labeling of cells in the differentiated zone, including some cells with abnormal bisbenzamide-stained nuclei (indicated by short arrows). Clusters of abnormal bisbenzamide-stained nuclei can be seen within phagocytes (indicated by arrows). Scale bars, 50 μm.

Table 1. Embryonic lethality of Bcl-x null mutation (*23*).

Age (days)	Number in litter	Total concept-uses	Number of normal-looking embryos	Genotype of normal embryos			Number of abnormal embryos*
				+/+	+/−	−/−	
E11.5-12.0	3	27	27	10	10	7	0
E12.5-13.0	4	37	36	13	16	7	1
E13.5-14.0	4	35	23	9	14	0	12
E14.5-15.0	1	10	9	3	6	0	1
E15.5-16.0	2	15	12	3	9	0	3

*All abnormal embryos were homozygous mutant (*bcl-x*$^{-/-}$) mice and had already died.

the increased neuronal death observed in the *bcl-x*$^{-/-}$ nervous system in vivo represents a primary event and is not simply secondary to the hematopoietic dysfunction described below.

To further define the degenerative changes observed in *bcl-x*$^{-/-}$ embryos, we stained sections of E12.5 mutant and wild-type mice by the terminal-deoxytransferase (TdT)–mediated deoxyuridine triphosphate (dUTP)–biotin nick end-labeling (TUNEL) method to identify apoptotic cells (*12*) (Fig. 3). In wild-type mice, occasional TUNEL-labeled nuclei were observed in the spinal cord and dorsal root ganglia. In comparison, mutant mice had an increase in the number of TUNEL-labeled nuclei in these sites, as well as in nonproliferative zones throughout the central nervous system (*8*). We also found a threefold increase in TUNEL-labeled nuclei in histologically identifiable hematopoietic cells in E12.5 *bcl-x*$^{-/-}$ liver compared to heterozygote and wild-type tissue (Fig. 3, C and D). To address the localization of *bcl-x* transcripts, we detected mRNA in E12.5 wild-type tissue sections by in situ hybridization (Fig. 4). Consistent with our findings that differentiating neurons in the intermediate zone and hematopoietic cells in the liver showed extensive apoptosis in *bcl-x*$^{-/-}$ mice, the *bcl-x* mRNA was expressed in those regions in wild-type mice. Because much of the observed cell death in the *bcl-x*$^{-/-}$ nervous system occurred prior to, or coincident with, terminal differentiation, it is unlikely that lack of target-derived neurotrophic factors or synaptic activity could account for the neuronal destruction. These findings suggest that programmed cell death in the developing brain and hematopoietic system is critically dependent on Bcl-x expression.

The lymphoid system is the second tissue where extensive apoptosis occurs and was found to be severely affected in the Bcl-2–deficient mice (*3*, *4*). Because of early embryonic lethality, we could not study the effect of Bcl-x absence on lymphocytes in the germline mutant mice. To study the function of Bcl-x in lymphocytes, we used the double-knockout method (*9*, *13*, *14*). We injected the *bcl-x*$^{-/-}$ ES or parental wild-type ES cells into the blastocysts from C57BL/6 (B6) and recombination activating gene–2 (RAG-2)–deficient mice to generate chimeric mice (B6 and RAG-2 chimeric mice, respectively).

In the chimeric mice, the maturation of *bcl-x*$^{-/-}$ T and B cells was reduced. In the thymus, there was a reduction in the proportion of mature CD4$^+$ or CD8$^+$ single positive (SP) thymocytes (Fig. 5A and Table 2). The thymocytes that did differentiate were derived from injected *bcl-x*$^{-/-}$ ES cells, as determined by Southern (DNA) blot analy-

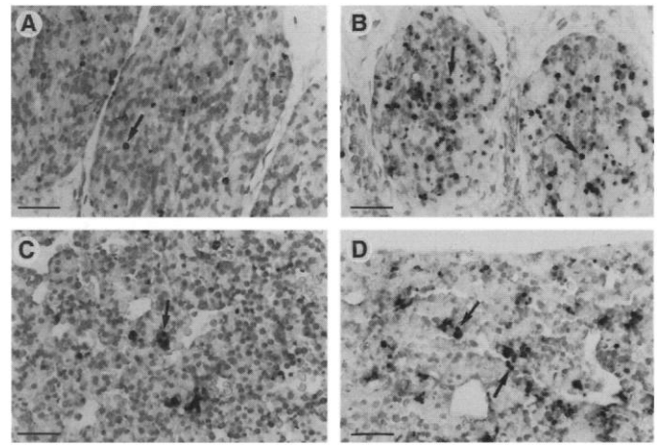

Fig. 3. TUNEL staining of E12.5 wild-type (A and C) and *bcl-x*$^{-/-}$ (B and D) dorsal root ganglia (A and B) and liver (C and D) (*26*). Scattered TUNEL-positive nuclei are seen in the wild-type dorsal root ganglia (**A**) and are greatly increased in the *bcl-x*$^{-/-}$ ganglia (**B**), which also appear shrunken. The frequency of TUNEL-positive nuclei in liver hematopoietic elements is low in wild-type mice (**C**) compared to *bcl-x*$^{-/-}$ mice (**D**). Scale bars, 50 μm.

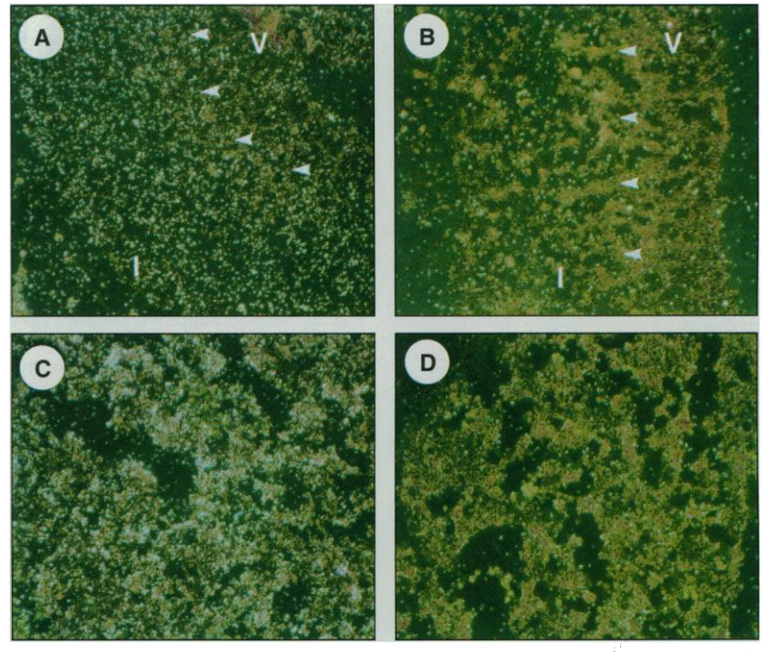

Fig. 4. In situ hybridizations of E12.5 wild-type (A and C) and *bcl-x*$^{-/-}$ (B and D) brain (A and B) and liver (C and D) (*27*). *bcl-x* mRNA was highly localized in the intermediate zone (labeled I) of the developing brain (**A**) and in the liver (**C**) of the wild-type mice. In comparison, *bcl-x*$^{-/-}$ mice had few grains similar to background level (**B** and **D**). Arrowheads indicate the border between ventricular (labeled V) and intermediate zones. Left side, intermediate zone; right side, ventricular zone.

Table 2. Proportion of lymphocyte populations in chimeric mice (*24*). Data show the proportion among Ly9.1$^+$ lymphocytes in B6 chimeric mice. SP, single positive; DP, double positive; BM, bone marrow; and LN, lymph node.

Genotype	Thymocytes		BM cells		LN cells		Splenocytes	
	SP	DP	B220$^+$IgM$^-$	B220$^+$IgM$^+$	T	B	T	B
Wild-type	21.8 ± 4.2 (n = 8)	73.3 ± 3.8 (n = 8)	50.8 ± 3.1 (n = 4)	26.2 ± 1.9 (n = 4)	63.0 ± 7.0 (n = 8)	33.3 ± 5.5 (n = 8)	64.4 ± 7.0 (n = 6)	21.0 ± 4.1 (n = 8)
bcl-x$^{-/-}$	14.3 ± 2.4 (n = 10)	78.4 ± 4.9 (n = 10)	27.8 ± 4.2 (n = 4)	10.0 ± 3.7 (n = 4)	58.2 ± 9.5 (n = 10)	30.4 ± 5.1 (n = 8)	39.4 ± 7.3 (n = 6)	14.1 ± 4.1 (n = 8)

sis (8, 15). In the bone marrow (BM), the proportion of mature B cells was reduced (Fig. 5B and Table 2). In the B6 chimeric mice, the proportion of $B220^{dull}IgM^-$ cells was decreased (Table 2). This decrease was not evident in the RAG-2 chimeric mice because $B220^{dull}IgM^-$ cells were also derived from RAG-2 blastocysts (14). Forward scatter parameter analysis (16) showed that small pre-B cells rather than the large pro-B cells in the $B220^{dull}IgM^-$ population were preferentially decreased in both the B6 and RAG-2 chimeric mice (Fig. 5C) (8). In contrast, lymph node (LN) and spleen cells of *bcl-x*$^{-/-}$ chimeric mice showed normal population distribution, although the ratios of mature T and B cells were decreased (Table 2). Thus, *bcl-x*$^{-/-}$ lymphocytes can differentiate into mature cells, although the total number of mature lymphocytes generated is decreased.

Thymocytes, BM, and LN cells were cultured for examination of in vitro life-span. Among thymocytes, *bcl-x*$^{-/-}$ TCR^{med} cells, but not TCR^{hi} cells, died more quickly than controls (Fig. 6, A and B). Most *bcl-x*$^{-/-}$ double-positive (DP) thymocytes disappeared during a 48-hour culture (Fig. 5A). The *bcl-x*$^{-/-}$ $B220^+$ BM cells behaved similarly (Fig. 6D). On the basis of staining patterns of B220 versus IgM or of B220 versus IgD (8), $B220^{dull}IgM^-$ and immature B cells ($B220^{dull}IgM^+IgD^-$ cells) were involved (Fig. 5B). However, life-spans of mutant LN T and B cells were comparable to those of controls (Fig. 6, C and E), whereas mature T and B cells in *bcl-2*$^{-/-}$ LN cells are mostly apoptotic (3, 4, 17). Thus, the absence of Bcl-x affects the life-span and apoptosis of developing immature lymphoid cells rather than of their mature counterparts, whereas in the *bcl-2*$^{-/-}$ mice this pattern is reversed (3, 4, 17).

The abnormality we observed in the lymphoid system is similar to that which occurs in c-*abl*–deficient mice (18). Similarly, the abnormalities found in the nervous and hematopoietic systems are similar to those observed in *rb*-deficient mice (19). In the *rb*-deficient mice, differentiating neurons die in the brain and spinal cord, and hematopoiesis in the liver is abnormal. However, unlike in *rb*$^{-/-}$ brain, increased mitosis was not observed in *bcl-x*$^{-/-}$ brain. The c-Abl protein interacts physiologically with Rb protein (20), and both may be involved in cell cycle controls (21, 22). These similarities and observations suggest the possibility of a functional connection between Bcl-x, c-Abl, and Rb.

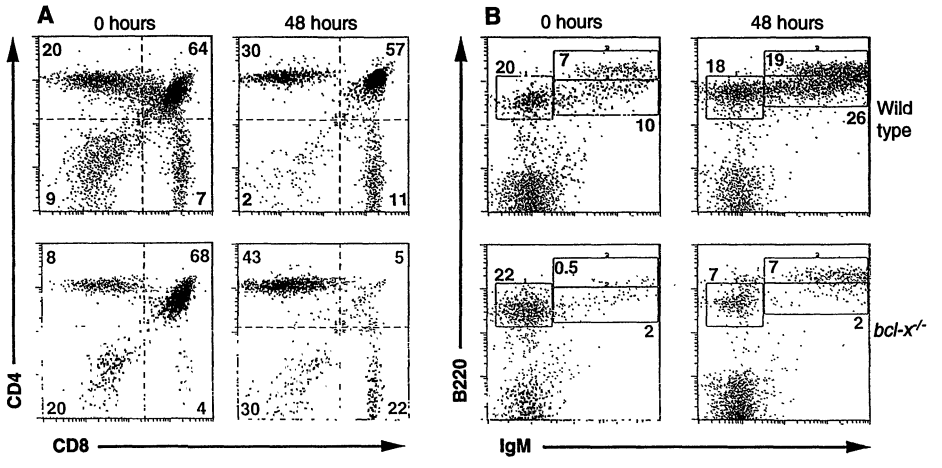

Fig. 5. Flow cytometric analysis of thymocytes and BM cells (24). Thymocytes (**A**) and BM cells (**B**) from control (upper panels) and *bcl-x*$^{-/-}$ RAG-2 chimeric mice (lower panels) were stained for CD4 and CD8 (A) or B220 and IgM (B) and analyzed before (left panels) and after (right panels) 48-hour culture. The $CD4^-CD8^-$ double negative (DN) population was increased in both wild-type and *bcl-x*$^{-/-}$ thymocytes because DN thymocytes contain the cells from RAG-2 blastocysts besides those from ES clones (14). BM cells (**C**) from control (left panel) and *bcl-x*$^{-/-}$ B6 chimeric mice (right panel) were gated on $Ly9.1^+B220^{dull},IgM^-$ population and cell size by forward scatter analysis.

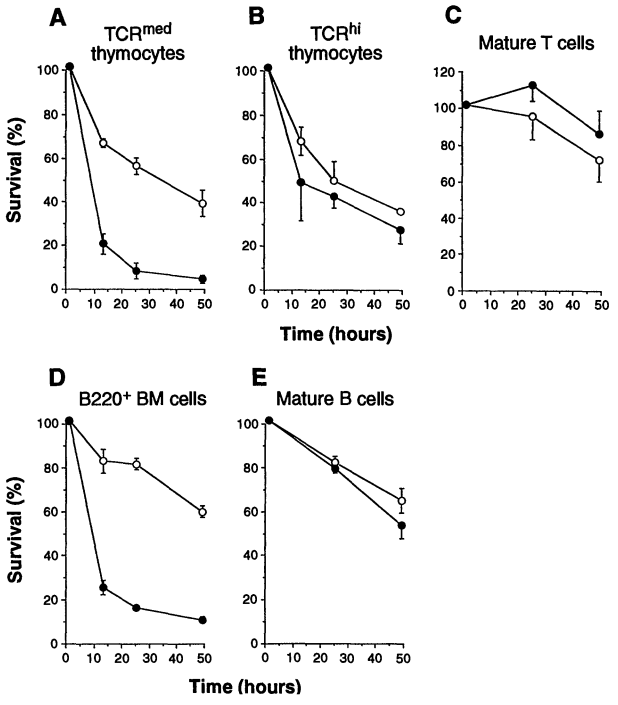

Fig. 6. In vitro cell survival of thymocytes and BM and LN cells. Assays were performed as described (3). TCR^{med} (**A**), TCR^{hi} thymocytes (**B**), LN T cells (**C**), $B220^+$ BM cells (**D**), and LN B cells (**E**) from *bcl-x*$^{-/-}$ (closed circles) and control (open circles) B6 chimeric mice were cultured for the indicated times. Experiments shown were done with three knockout and three control chimeras. Experiments were also performed with chimeras derived from different independent ES cell lines with similar results.

REFERENCES AND NOTES

1. D. L. Vaux, *Proc. Natl. Acad. Sci. U.S.A.* **90**, 786 (1993); E. Cuende *et al.*, *EMBO J.* **12**, 1555 (1993); T. E. Allsopp, S. Wyatt, H. F. Paterson, A. M. Davies, *Cell* **73**, 295 (1993); A. Batistatou, D. E. Merry, S. J. Korsmeyer, L. A. Greene, *J. Neurosci.* **13**, 4422 (1993); L.-T. Zhong *et al.*, *Proc. Natl. Acad. Sci. U.S.A.* **90**, 4533 (1993); M. Dubois-Dauphin, H. Frankowski, Y. Tsujimoto, J. Huarte, J.-C. Martinou, *ibid.* **91**, 3309 (1994).
2. D. M. Hockenbery, M. Zutter, W. Hickey, M. Nahm, S. J. Korsmeyer, *Proc. Natl. Acad. Sci. U.S.A.* **88**, 6961 (1991); D. P. LeBrun, R. A. Warnke, M. L. Cleary, *Am. J. Pathol.* **142**, 743 (1993); D. Veis-Novack and S. J. Korsmeyer, *Ibid.* **145**, 61 (1994); D. E. Merry, D. J. Veis, W. F. Hickey, S. J. Korsmeyer, *Development* **120**, 301 (1994).
3. K.-i. Nakayama *et al.*, *Science* **261**, 1584 (1993).
4. K. Nakayama *et al.*, *Proc. Natl. Acad. Sci. U.S.A.* **91**, 3700 (1994); D. J. Veis, C. M. Sorenson, J. R. Shutter, S. J. Korsmeyer, *Cell* **75**, 229 (1993).
5. G. T. Williams and C. A. Smith, *Cell* **74**, 777 (1993); E. Y. Lin, A. Orlofsky, M. S. Berger, M. B. Prystowsky, *J. Immunol.* **151**, 1979 (1993).
6. L. H. Boise *et al.*, *Cell* **74**, 597 (1993).
7. M. Gonzalez-Garcia *et al.*, *Development* **120**, 3033 (1994); W. Fang, J. J. Rivard, D. L. Mueller, T. W. Behrens, *J. Immunol.* **153**, 4388 (1994); S. Krajewski *et al.*, *Cancer Res.* **54**, 5501 (1994).
8. N. Motoyama, K. A. Roth, D. Y. Loh, unpublished observations.
9. Genomic DNA containing the *bcl-x* locus was isolated from a library of mouse strain 129 DNA (Strat-

agene). A 1.8-kb Xho I–Bam HI fragment containing most of the Bcl-x coding region was replaced with either a PGK-*neo* polyadenylate [poly(A)] cassette or a PGK-*hyg* poly(A) cassette. The targeting vectors, pXKO-NEO and pXKO-HYG, contain a 6.0-kb region of homology 5′ and 1.0 kb 3′ of the drug-resistance markers and a PGK-*tk* poly(A) cassette. Transfections and selections were performed as described (*3*). DNAs prepared from ES cells were digested with Eco RV, transferred to a nylon membrane, and then hybridized with the 0.4-kb Kpn I–Pst I probe that flanked the 3′ homology region. Expected sizes for wild-type *bcl-x*, mutant *bcl-x* by pXKO-NEO, and mutant *bcl-x* by pXKO-HYG are 9.8, 7.0, and 5.5 kb and were detected in wild-type, *bcl-x*$^{+/-}$, and *bcl-x*$^{-/-}$ ES clones, respectively.
10. R. W. Oppenheim, *Annu. Rev. Neurosci.* **14**, 453 (1991).
11. B. Riederer and A. Matus, *Proc. Natl. Acad. Sci. U.S.A.* **82**, 6006 (1985); R. P. Tucker, L. I. Binder, A. I. Matus, *J. Comp. Neurol.* **271**, 44 (1988).
12. Y. Gavrieli, Y. Sherman, S. A. Ben-Sasson, *J. Cell Biol.* **119**, 493 (1992).
13. A. Jakobovits *et al.*, *Proc. Natl. Acad. Sci. U.S.A.* **90**, 2551 (1993).
14. J. Chen, R. Lansford, V. Stewart, F. Young, F. W. Alt, *ibid.*, p. 4528; J. Chen *et al.*, *Immunity* **1**, 65 (1994).
15. ES-derived thymocytes were purified with an antibody to CD8 (anti-CD8) and magnetic beads from *bcl-x*$^{-/-}$ or wild-type RAG-2 chimeric mice as described (*3*). DNAs prepared from the purified CD8-positive thymocytes were subjected to Southern blot analysis as described above.
16. D. Kitamura *et al.*, *Cell* **69**, 823 (1992).
17. K.-i. Nakayama, K. Nakayama, L. B. Dustin, D. Y. Loh, in preparation.
18. V. L. J. Tybulewicz, C. E. Crawford, P. K. Jackson, R. T. Bronson, R. C. Mulligan, *Cell* **65**, 1153 (1991); P. L. Schwartzberg *et al.*, *ibid.*, p. 1165.
19. E. Y.-H. P. Lee *et al.*, *Nature* **359**, 288 (1992); T. Jacks *et al.*, *ibid.*, p. 295; A. R. Clarke *et al.*, *ibid.*, p. 328.
20. P. J. Welch and J. Y. J. Wang, *Cell* **75**, 779 (1993).
21. D. W. Goodrich, N. P. Wang, Y.-W. Qian, E. Y.-H. P. Lee, W.-H. Lee, *ibid.* **67**, 293 (1991).
22. C. L. Sawyers, J. McLaughlin, A. Goga, M. Havlik, O. Witte, *ibid.* **77**, 121 (1994).
23. One of four *bcl-x*$^{-/-}$ mice at E12.5 and two E13.5 *bcl-x*$^{-/-}$ mice were examined histologically and showed autolytic changes throughout the embryonic tissues indicative of intrauterine death. Careful examination of the three viable E12.5 *bcl-x*$^{-/-}$ embryos showed no obvious gross fetal abnormality, and histologic examination of two E12.5 *bcl-x*$^{-/-}$ placentas showed normal maternal and fetal components. In the embryonic mouse, yolk-sac–derived nucleated red blood cells begin to disappear from the circulation around E12, when the liver becomes the principal source of hematopoietic activity [M. H. Kaufmann, *The Atlas of Mouse Development* (Academic Press, San Diego, CA, 1992), p. 128]. Because the *bcl-x*$^{-/-}$ mice were paler, died at approximately E13, and showed a marked increase in TUNEL-labeled nuclei in the hematopoietic elements of the liver, it is possible that a defect in hepatic hematopoiesis, coupled with declining numbers of yolk sac–derived red cells, produces hypoxic damage to the embryo, resulting in death.
24. Thymocytes and BM and LN cells (1×10^6 cells each) were prepared from wild-type and *bcl-x*$^{-/-}$ B6 chimeric mice and were stained with anti-Ly9.1–fluorescein isothiocyanate (FITC), and anti-CD4–phycoerythrin (PE) and anti-CD8–biotin, or anti-B220–PE and anti-immunoglobulin M (IgM)–biotin (PharMingen). For RAG-2 chimeric mice, cells were stained with anti-CD8–FITC and anti-CD4–PE, or anti-IgM–FITC or anti-IgD–FITC (Southern Biotechnology) and anti-B220–PE. Biotin conjugate was revealed by RED 613-streptavidin (Gibco BRL). Dead cells were excluded by staining with propidium iodide (Boehringer Mannheim). Flow cytometric analysis was done on FACScan computer and software (Becton Dickinson).
25. Whole embryos were fixed in 4% paraformaldehyde and embedded in paraffin, and 5-μm-thick sagittal sections were cut at multiple levels. Sections were alternatively stained with hematoxylin-eosin and with cresyl violet. Unstained sections were processed for immunostaining as described [M. L. Hermiston, C. B. Latham, J. I. Gordon, K. A. Roth, *J. Histochem. Cytochem.* **40**, 1283 (1992)]. A mouse monoclonal antibody to MAP2 (Sigma) was used at a dilution of 1:1000 to detect differentiating neurons. Primary antibodies were detected with a CY-3-conjugated donkey antiserum to mouse IgG (Jackson Immunoresearch Laboratories). Omission of the primary antibody resulted in only weak, nonspecific labeling of the blood vessels. After immunolabeling, sections were incubated for 10 min at room temperature in bisbenzamide (0.04 μg/ml) (Hoechst 33258, Sigma) to label cell nuclei. Slides were viewed and photographed with a Zeiss Axioskop fluorescence microscope.
26. Apoptotic cells were identified by the TUNEL method (*12*) modified to detect incorporated digoxygenin-dUTP with either alkaline phosphatase or gold-conjugated sheep antibody to digoxygenin.
27. In situ hybridizations were performed as described [H. Sawa, B. E. Sobel, S. Fujii, *Circ. Res.* **73**, 671 (1993)]. For construction of RNA probes, pBluescript SKII+ plasmid containing a 0.8-kb mouse *bcl-x* complementary DNA insert was linearized by restriction digestion with Xho I or Not I (for antisense and sense, respectively) and transcribed with T7 or T3 RNA polymerase in the presence of ^{35}S-labeled uridine triphosphate (UTP).
28. We thank F. W. Alt for RAG-2–deficient mice, P. Mombaerts for E14 ES cell line, J. Y. J. Wang for helpful suggestions, and L. B. Dustin and I. T. Chan for critical reading of the manuscript. Supported by the Howard Hughes Medical Institute (D.Y.L.) and the Japan Society for the Promotion of Science (N.M.).

2 November 1994; accepted 9 February 1995

Synaptic Desensitization of NMDA Receptors by Calcineurin

Gang Tong,* Dawn Shepherd, Craig E. Jahr†

Desensitization is a phenomenon that is common to many ligand-gated ion channels but has been demonstrated only rarely with physiological stimulation. Numerous studies describe desensitization of the *N*-methyl-D-aspartate (NMDA) subtype of glutamate receptor by exogenous agonists, but whether synaptic stimulation causes desensitization has been unknown. Synaptic stimulation of NMDA receptors on rat hippocampal neurons resulted in desensitization that was prevented by intracellular 1,2-bis(*o*-aminophenoxy)ethane-*N*,*N*,*N*′,*N*′-tetraacetic acid (BAPTA), adenosine-5′-*O*-(3-thiotriphosphate) (ATP-γ-S), or inhibitors of phosphatase 2B (calcineurin), but not by inhibitors of phosphatases 1 and 2A or of tyrosine phosphatases. Synaptic NMDA receptors may fluctuate between phosphorylated and dephosphorylated forms, depending on the rate of synaptic stimulation and the magnitude of the associated influx of calcium through NMDA receptors.

The magnitude of Ca^{2+} influx through synaptically activated NMDA receptor channels not only affects the amplitude and lifetime of long-term synaptic plasticity at certain central synapses, but also is a factor in whether subsequent synaptic strength is increased or decreased (*1–3*). Several species of protein phosphatases cause diminished NMDA channel activity (*4–6*), which may result in decreased Ca^{2+} influx during synaptic stimulation. In addition, calcineurin activity stimulated by brief elevations of intracellular Ca^{2+} concentration (*7*) causes the development of a glycine-insensitive form (*8, 9*) of NMDA receptor desensitization. Because NMDA receptor channels are very permeable to Ca^{2+} (*10*), synaptic activation may enable this form of desensitization and may result in a negative feedback of NMDA receptor synaptic activation. If desensitization is enhanced by synaptic stimulation, the decrease in ion flux will result in smaller intracellular Ca^{2+} transients that could shift the balance between long-term potentiation (LTP) and long-term depression (LTD) of synaptic strength (*1–3*).

Isolated cultured rat hippocampal neurons make synapses onto themselves (*11*) and were used to measure NMDA receptor desensitization induced by synaptic stimulation. The synapses were conditioned by stimulating them four times within 75 ms (*12*) and were tested with a single stimulus after a variable interval (0.8 to 7.5 s). The depression of the test excitatory postsynaptic current (EPSC) relative to the first conditioning EPSC could result from a combination of a lower presynaptic release probability (synaptic depression or presynaptic inhibition) and a decreased sensitivity of postsynaptic receptors (desensitization). The amount of depression resulting from NMDA receptor desensitization was estimated by comparing the amplitudes of test EPSCs conditioned by the four-pulse conditioning stimulus delivered in the presence or absence of the competitive antagonist of the NMDA receptor, D-2-amino-5-phosphonopentanoic acid (D-AP5, 100 μM) (Fig. 1A). In the presence of D-AP5, glutamate released by

G. Tong and C. E. Jahr, Vollum Institute and Department of Cell Biology and Anatomy, Oregon Health Sciences University, Portland, OR 97201–3098, USA.
D. Shepherd, Vollum Institute, Oregon Health Sciences University, Portland, OR 97201–3098, USA.

*Present address: Department of Pharmacology, University of California, San Francisco, CA 94143, USA.
†To whom correspondence should be addressed.